THREE-DIMENSIONAL STRUCTURES OF N_2-DILUTED STOICHIOMETRIC H_2-O_2 FLAMES IN NARROW CHANNELS

Y. Ballossier, F. Veiga-López, F. Virot, J. Melguizo-Gavilanes

Institute Pprime, UPR 3346 CNRS, ISAE-ENSMA, 86961, Futuroscope-Chasseneuil, France

Abstract

Flame propagation and acceleration in unobstructed channels/tubes is usually assumed as symmetric. A fully optically accessible narrow channel that allows to perform simultaneous high-speed *schlieren* visualization from two mutually perpendicular directions was built to asses the validity of the aforementioned assumption. Here, we provide experimental evidence of the interesting three-dimensional structures and asymmetries that develop during the acceleration phase and show how these may control detonation onset in N_2-diluted stoichiometric H_2-O_2 mixtures.

1. INTRODUCTION

Hydrogen-oxygen chemical reactions (e.g., combustion, fuel cells) release large amounts of energy and only produce water as products. With a low energy density per volume, and high explosive potential, hydrogen storage and handling are the main technological constrains for its widespread safe use. Indeed, in case of leak, hydrogen can mix with air and accidentally ignite in the presence of an ignition source (e.g., hot surface or electrical spark) posing a serious safety hazard. In confined geometries, even without obstacles, the resultant flames may accelerate and potentially transit to detonation [1, 2]; a more destructive combustion mode that may cause large structural damage. Understanding the physical mechanisms that drive the transition is thus key to avoiding the disastrous onset of detonation fronts.

General deflagration-to-detonation transition (DDT) events in unobstructed channels take place in distinct stages [2, 3], comprising the initial flame kernel that corrugates and quickly accelerates producing pressure waves ahead of itself, as well as the onset of precursor shocks that compress the fresh mixture leading to the initiation of a detonation wave upon complex interactions among flames, shocks and hydrodynamic boundary layers. Recent numerical research on DDT [4, 5] confirm the aforementioned mechanisms emphasizing the importance of viscous heating and/or local pressure increments close to the flame front as crucial components of the DDT process.

Numerical studies typically demand simplifications to make them tractable. One of the most commonly exploited is the use of axial symmetries to reduce resolution requirements [6–8]. However, to the best of our knowledge, this reasonable but rather strong assumption is not supported by experimental evidence. Here, we present new experimental data on flame acceleration and detonation onset for stoichiometric H_2-O_2 mixtures at ambient conditions and different degrees of N_2 dilution, recorded from two different perspectives, which allow us to assess three-dimensional effects during the entire DDT process.

The paper is structured as follows: section 2 introduces a novel experimental setup, which allows complete optical access for simultaneous *schlieren* visualization from two mutually perpendicular directions

along an almost 1-m-long channel. Next, we discuss the main findings of the experiments in section 3 highlighting the very distinct topologies observed as the DDT evolution is followed from ignition to detonation onset. Finally, concluding remarks and future work are presented in section 4.

2. EXPERIMENTAL SETUP

2.1. Apparatus and procedure

Figure 1 sketches the experimental setup used. N_2-diluted hydrogen-oxygen flames propagate through a 1030-mm × 10-mm × 9.4-mm channel whose cross section's geometric uniformity is ensured by means of retaining walls of 0.6-mm height (see detail in Fig. 1-*left*). The channel walls are 15-mm-thick polycarbonate plates enclosed by aluminum flanges at the top and bottom together with lateral spacers on the sides, to avoid bending during detonation onset and subsequent propagation. The structural integrity of the channel is guaranteed with bolts screwed on the aluminum frame in a sandwich-like configuration. Regarding the boundary conditions, the channel is kept closed at the ignition end and left open at the opposite end (Fig. 1-*left*).

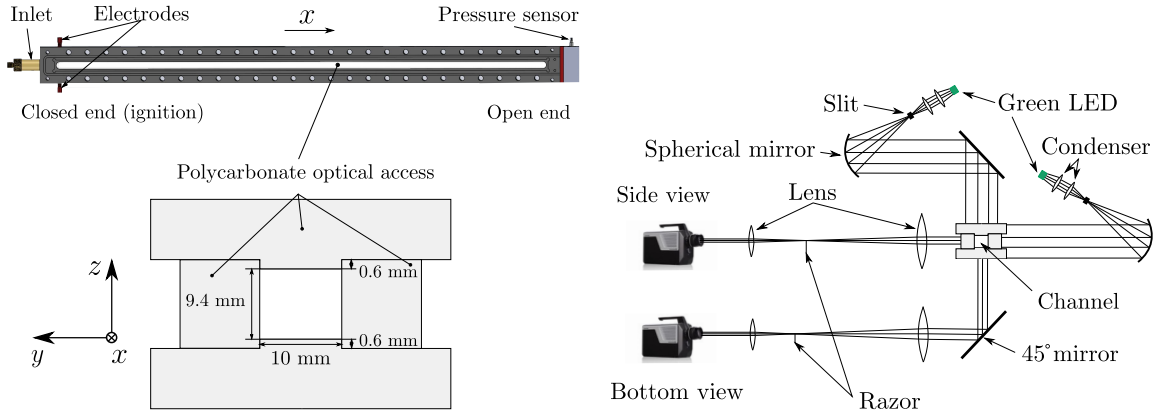

Figure 1: *Left:* Sketch of the narrow channel used as a combustion chamber (top) and cross-sections without the aluminum flanges (bottom). *Right:* Schematic of the visualization directions. 'Side' and 'Bottom' views refer to the position of the cameras. Condenser: 50.8 mm-diameter lens; Collimator: 75 mm-diameter spherical mirrors; Focalization: 75 mm-diameter lens; Collection: 50-mm diameter lens.

The experiments are conducted as follows: (i) the channel is first vacuumed to an absolute pressure below 10 mbar (controlled by a MKS 220DA pressure sensor); (ii) a plastic cap, held by a servo motor's arm, seals the open end of the channel; (iii) the reactive mixture (prepared and mixed beforehand) is fed into the channel until atmospheric pressure is reached. At this point, the plastic cap is automatically removed by the servo motor; (iv) one second later, the mixture is ignited 3 mm from the closed end by the electric arc that forms between the two electrodes whose estimated energy, E_{ign}, is approximately 1 mJ). This procedure ensures adequate control of the mixture equivalence ratio ($\Phi = 1 \pm 0.01$) within the channel. In addition, the waiting time between filling and ignition is controlled to never exceed 15 s as this was found to avoid any impact of initial flow unsteadiness on the early stages of flame propagation [9]; (v) to remove any visible condensation from the burned gases the channel is vacuumed for at least three minutes after each test.

2.2. Diagnostics

High-speed simultaneous *schlieren* visualization requires a complete independent set of optics for the two cameras used: (i) a Shimadzu HPVX-2 (bottom view), with acquisition rates ranging from 200,000 (200 ns exposure time) to 10 million fps (50 ns exposure time), and (ii) a Shimadzu HPV-2 (side view) with acquisition rates of 125,000 (1000 ns exposure time) to 1 million fps (250 ns exposure time). Table 1 summarizes the optical configuration shown in Fig. 1-*Right*. The optical layout allows for resolutions of 111 μm/pixel and 106 μm/pixel to visualize 34.6 mm (side) and 42.5 mm-long (bottom) sections, respectively. The resolutions are 312 pixels horizontal and 90 pixels vertical for both views, to match the smallest field of view. Cameras are from different generations, resulting in discrepancies in sensitivity and level of details provide on different views. A complete characterization of the flame acceleration dynamics is carried out by keeping the optics fixed and translating the channel. At least two test per section and per dilution were performed to assess repeatability. Additionally, due to the intense chemiluminescence during detonation onset, hard-coated short-pass filters (Thor Labs Ref. FESH0550) were used between the set of collector lenses and the high-speed cameras; with a cut-off wavelength below 400 nm and above 550 nm, the filters do not affect the acquired images from the LED's emission but avoid saturation of the cameras' sensors.

Table 1: Optical focal lengths in mm for both visualization directions.

View	Condenser	Slit	Razor	Collimator	Focalization	Collection
Side	75 / 150	90°	90°	500	500	150
Bottom	75 / 150	90°	90°	500	500	300

Both high speed cameras are triggered from the signal emitted by a photo-diode (BPW34) placed at the start of the section tested. A global view of the channel was also acquired for some tests using a third-camera (Photron SA-5), set at 165,000 fps and 1 μs exposure time, to collect run-up distances, i.e., distance from ignition to detonation onset.

3. RESULTS AND DISCUSSION

With the setup and detailed procedure described above, 214 tests for four nitrogen dilutions were performed to achieve the main goal of this work: to provide experimental evidence of the asymmetries present during flame acceleration and their influence on DDT onset. Table 2 lists properties such as the laminar burning velocity, S_L, expansion ratio, $\sigma = \rho_0/\rho_b$, Zel'dovich number, $\beta = E_a/R_u T_b(T_b - T_0)/T_b$, and steady detonation propagation velocity, D_{CJ}, for all the mixtures tested. The reported values were computed using Cantera [10] and the Shock and Detonation Toolbox [11] with the detailed mechanism of Mével [12, 13]. The methodology used to determine the effective activation energy E_a/RT_b can be found in [14]. In the expressions above ρ, T and R_u are the mixture density and temperature, and universal gas constant, respectively; subscripts 0 and b refer to fresh and burnt mixture. Also included in Table 2 is whether or not DDT occurred in our 1-m long channel.

3.1. Three dimensional structures during flame acceleration

The figures below show the flame dynamics obtained during our experimental campaign. Each frame is composed of two sub-frames including the 'Side' (xz-plane) and 'Bottom' (xy-plane) views. The

Table 2: Properties of the N_2-diluted stoichiometric H_2-O_2 mixtures studied. Initial conditions: p_0 = 100 kPa, T_0 = 300 K and $2H_2+O_2+\eta N_2$.

η	% $N_{2,vol}$	S_L (m/s)	σ	β	D_{CJ} (m/s)	DDT onset
0	0	10.4	8.25	2.6	2834	Yes
2	40	4.36	7.55	2.8	2184	Yes
2.5	45.5	3.64	7.35	3.3	2110	Yes
3.76	55.6	2.39	6.79	4.2	1968	No

horizontal axis displays the section along which the simultaneous visualization is performed, and the time stamps above each frame indicate the time elapsed from ignition. Unless otherwise stated, to obtain similar gray-scales in the figures, the raw images recorded with both cameras were post-processed by matching their histograms and resolution; performing a frame-by-frame subtraction of the average field obtained over the sequence collected; followed by a color inversion. The aforementioned steps were automated via a *Python* script, and the leftover noise ahead of the reacting fronts was manually removed. The final images were carefully checked and compared with the original videos afterwards to ensure that no artifacts were mistakenly produced as a result of our post-processing scheme.

3.1.1. Early stages

Figure 2 shows the flame topologies observed during early stages of flame propagation for $\eta = 0$ and $\eta = 3.76$ where η is the number of N_2 moles added to a stoichiometric H_2-O_2 mixture (i.e., $2H_2+O_2+\eta N_2$).

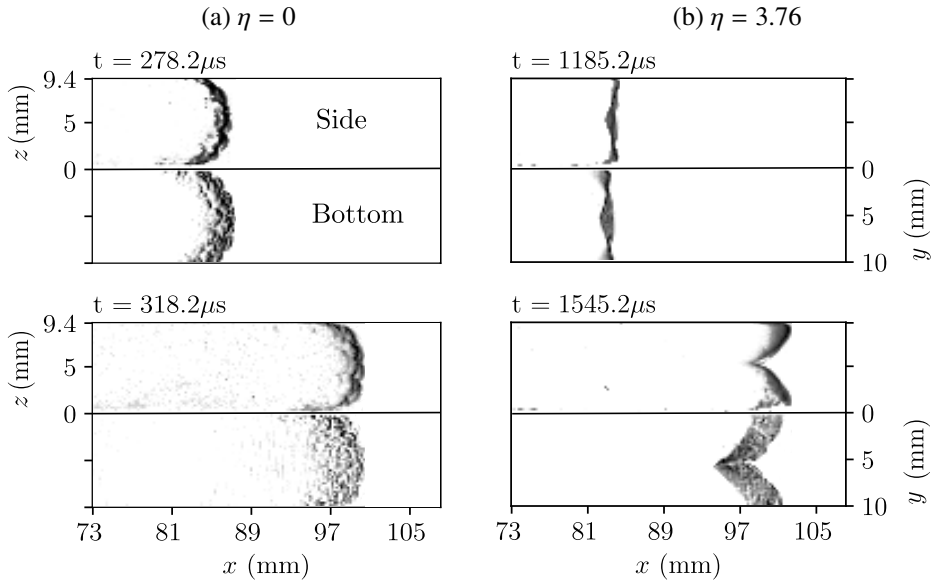

Figure 2: Simultaneous *schlieren* visualization of $2H_2+O_2+\eta N_2$ mixtures traveling through a visible section located between 73-107 mm from the closed end. t indicates the time elapsed from ignition.

Once ignited at the center of the channel, near the close end, spherical flame kernels propagate due to the combined effect of fresh reactants consumption, burnt products expansion and geometrical confinement. Regarding the latter, the presence of a closed end wall promotes a pressure build up that pushes the

flames towards the open end, increasing their surface area, associated consumption rates and therefore, results in their abrupt acceleration. Laminar finger-flame topologies [15–19] are observed for $x < 73$ mm (not shown).

For no N_2 dilution ($\eta = 0$), small scale Darrieus-Landau instabilities develop on the flame surface, resulting in larger overall burning rates than for $\eta = 3.76$, which prevents undiluted flames from inverting into a tulip flame. The inversion process is nicely depicted in Fig. 2 (b) which has been argued to be mostly driven by hydrodynamics [20].

Two-direction visualization confirms the symmetry of the flames during the first stages of propagation, as well as the development of instabilities as the main mechanism that increases the flame surface for $\eta = 0$, whereas flame inversion, after the front becomes flat, is a characteristic feature of cases that contain N_2. Intermediate dilutions, $\eta = 2$ and $\eta = 2.5$, show similar topologies and behaviors as $\eta = 3.76$, except that front flattening and inversion occur earlier, namely, at ~ 643 μs and ~ 777 μs, respectively.

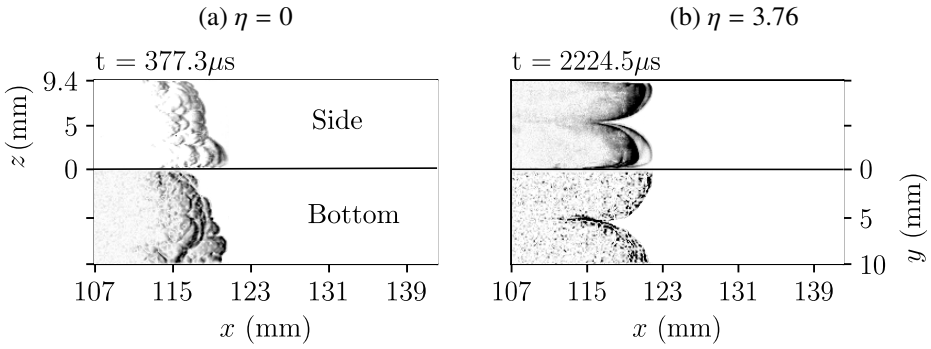

Figure 3: Simultaneous *schlieren* visualization of $2H_2+O_2+\eta N_2$ mixtures traveling through a visible section located between 107 and 140 mm from the closed end. t indicates the time elapsed from ignition.

Figure 3 shows the following section of the channel, $107 \leq x \leq 140$ mm, for the same dilution levels as in Fig. 2. As mentioned above for $\eta = 0$ the flame surface instabilities prevented flame inversion, but not its gradual flattening before developing asymmetries (see Fig. 3 (a)). The side view at $t = 377.3$ μs suggests that the flame propagates faster along the wall - $z = 0$ mm. The bottom view provides additional information and reveals its true topology: the flame propagates preferentially in a corner. This is the beginning of a form of inversion for this mixture. Instead of presenting the characteristic 'tulip shape' when observed from both planes the flame propagates faster near walls. For $\eta = 3.76$ the side view shows four distinct lobes burning near walls. The bottom view allows to pinpoint the exact location of the lobes to the corners (see Fig. 3 (b)) leaving the neighborhood of the channel's centerline with unreacted mixture. The extent of the latter increases as the flame moves towards the open end up until one/a few lobe(s) remain. These asymmetries arise earlier with less diluted mixtures ($\eta = 2.0$ and 2.5) and become predominant further downstream.

The next section of the channel, $140 \leq x \leq 174$ mm, is shown in Fig. 4 and displays very interesting three-dimensional dynamics for all dilutions considered. For $\eta = 0$ at $t = 431.8$ μs the side view exhibits an almost flat flame surface but the bottom view shows significant curvature along the y-axis. A similar topology as that just described is visible at $t = 459.8$ μs for both visualization directions, significant asymmetries are present with unreacted mixture trapped between the walls and the flame surface forming lobes along which intrinsic small scale instabilities continue to develop. The continuous presence of this 'tail' of fresh mixture and its growth is visible in subsequent frames ($t = 459.8 - 487.8$ μs). We emphasize that the extra information gathered by having simultaneous optical access allows us to unravel the complex flame topology at hand, and determine that the flame burns asymmetrically along the wall.

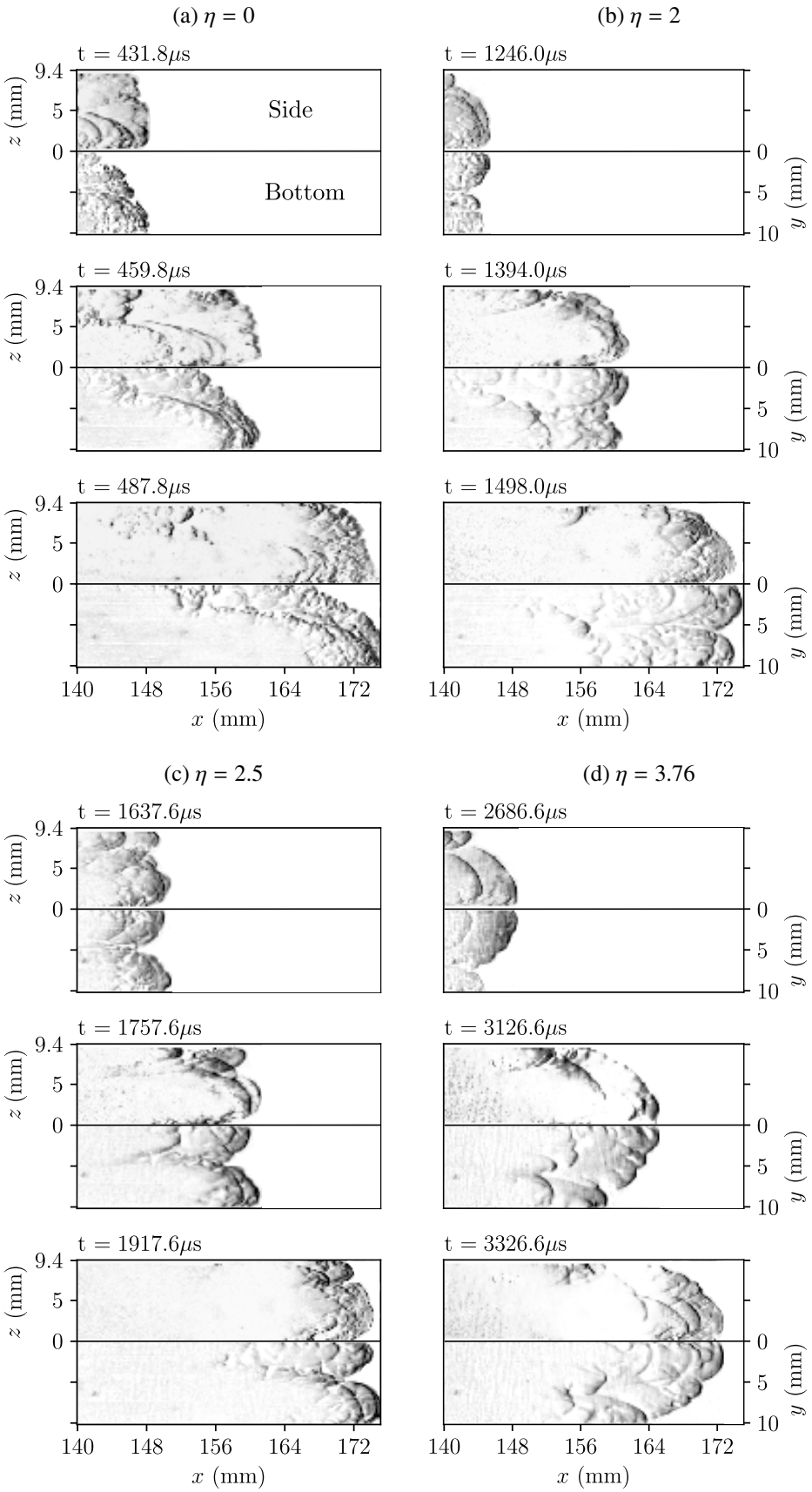

Figure 4: Simultaneous *schlieren* images of $2H_2$+O_2+ηN_2 mixtures traveling through a visible section located between 140 to 174 mm from the closed end. t indicates the time elapsed from ignition.

Remnants of such inversion are also visible for increasing N_2 dilution (Figs. 4 (b) and (c) – bottom view). The side view for $\eta = 2$ and 2.5 at t = 1246 μs and 1637.6 μs, respectively, exhibit preferential burning close to the bottom wall. Small lobes are visible on the top wall, but these are either consumed/absorbed by the growing reaction front coming from the bottom wall (see Fig. 4 (b); $t > 1394$ μs), or mixed into a convoluted wrinkled flame (see Fig. 4 (c); $t > 1757.6$ μs). For $\eta = 3.76$, the side views display similar structures as those for $\eta = 2$, except that smaller length scales are present on the flame surface for the latter; this is because for lower expansion ratios, σ, Darrieus-Landau instabilities are weaker. Again, note that had we only had access to the the side views of Figs. 4 (b) and (d) would have lead to the conclusion that increasing dilution had a minor influence on the large scale flame topologies. However, the bottom views shows a completely different picture, unequivocally proving that the break up of inversion described earlier takes place preferentially within a corner instead of uniformly spread over a wall.

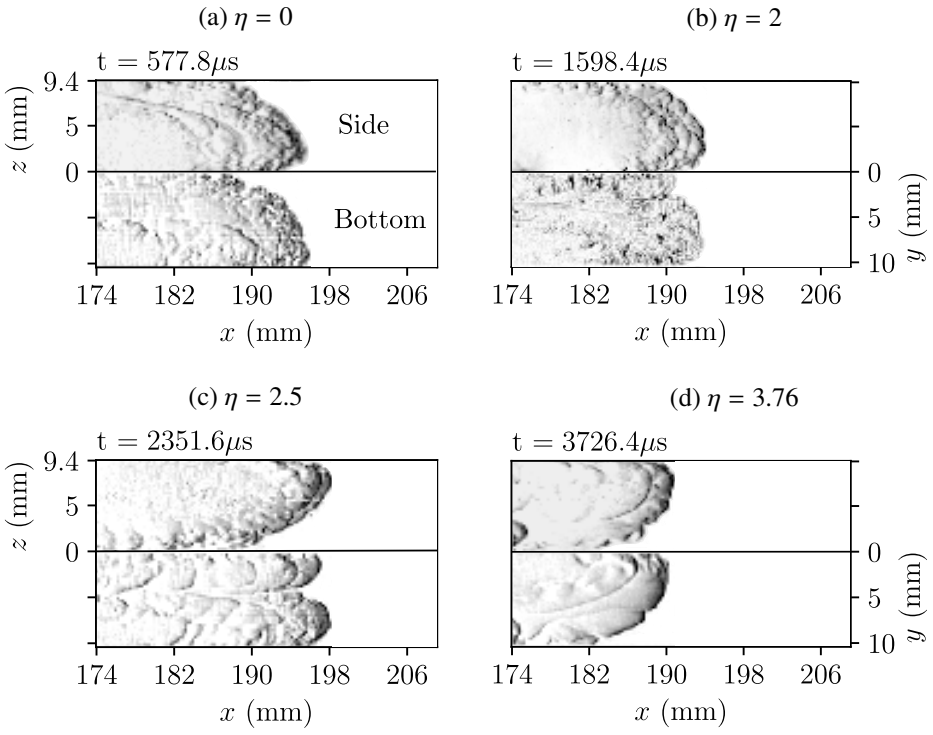

Figure 5: Simultaneous *schlieren* images of $2H_2+O_2+\eta N_2$ mixtures traveling through a visible section located between 174 to 208 mm from the closed end. t indicates the time elapsed from ignition.

Figure 5 shows the section $174 \leq x \leq 208$ mm for all N_2 dilutions considered. The flames do not seem to evolve significantly as they cross over this section of the channel. As a result, only one time instance is presented. In spite of the differences described above as a function of dilution for the previous section, the flame topologies are quite similar in this case. All frames exhibit distinct lobes and asymmetric propagation. Interestingly, the wall along which the flame propagates is different for $\eta = 0$ and 2 ($z = 0$ mm), than for $\eta = 2.5$ and 3.76 ($z = 9.4$ mm).

Section $208 \leq x \leq 243$ mm is shown in Fig. 6 only for $\eta = 0$ and 3.76 since all dilutions continue to display comparable shapes, namely curved and corrugated flame surfaces propagating away from the channel's center-line in the direction of a corner. Only flames without N_2 dilution ($\eta = 0$) entrain appreciable amounts of unreacted gas within the flame surface and walls. These highly stretched flame surfaces enhance flame acceleration and formation of pressures waves ahead of themselves. Up until

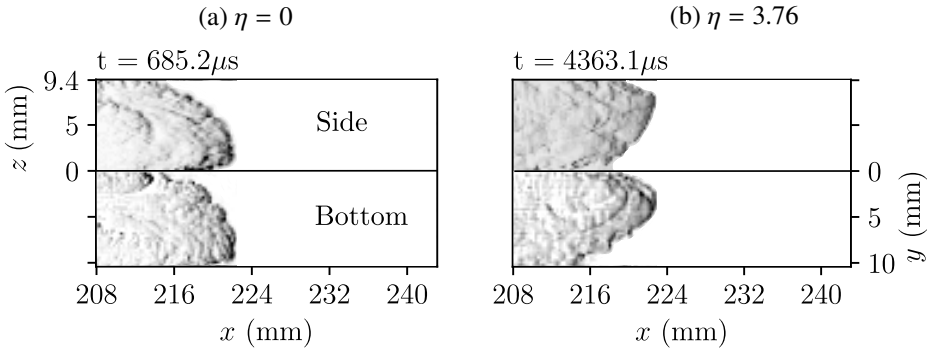

Figure 6: Simultaneous *schlieren* shots of $2H_2$+O_2+ηN_2 mixtures traveling through a visible section located between 208 to 243 mm from the closed end. t indicates the time elapsed from ignition.

transition to detonation takes place, all dilutions have similar overall topologies to those shown in Fig. 6.

3.1.2. DDT onset

To highlight important flow features during DDT onset such as the formation of pressure waves ahead of the flame surface, the post-processing scheme used for the figures shown in this section changed. We only matched their histograms and performed a contrast enhancement step. Figures 7 and 8 show detonation onset sequences for $\eta = 0$ whereas Fig. 9 does so for $\eta = 2$. While for $\eta = 2.5$ transition to detonation did occur within our channel, it systematically took place close to the outlet hence outside of the optically accessible area.

Note that the overall flame shape remains unchanged when comparing Fig. 6 (a) and Fig. 7 (a) although it has traveled over 104 mm between the frames. The region filled with unburned mixture has shifted from the corner to the center of the channel, shrinking along the channel's width, but growing along its length, in a similar shape to the *waffle cone*-like structure described in [21] for round tubes with larger cross-sections. The acceleration process leads to the formation of pressure waves ahead of the flame, pre-heating and pre-compressing the reactive mixture [3]. This mechanism provides a positive feedback to further enhance the acceleration of the flame, during which it gradually catches up with the aforementioned precursor shocks. As the flame gains ground within the preheated zone (see Fig. 7; t = 737.2 μs), the favorable thermodynamic conditions are achieved for the mixture to ignite in the subsequent frame at t = 743.2 μs. The spherical blast wave that results from the explosion process overtakes the preheated zone, interacts with the flame and the unreacted mixture entrained between its surface and the walls to finally couple with the leading pre-cursor shock to form a detonation wave. Surprisingly, the side and bottom views do not show obvious differences and could almost be overlaid, but asymmetries in flame topologies continue to be present. An interesting example of the advantages of two-direction visualization is the ability to pinpoint the exact location of the detonation onset: at a corner. While it appears to have taken place behind the flame tip, ignition of the mixture actually occurs at the edge of the flame (see Fig. 7 at t = 743.2 μs). Our results suggests that detonation onset seems to be provoked by flame interactions with the multitude of shocks trapped between the flame, the channel's walls and the leading precursor shock. We note that the DDT point is observed to be preferentially located within corners, but not always at the same corner. Viscous heating close to the walls may plausibly setup a temperature gradient within the boundary layers making these areas favorable to detonation initiation, the so-called Zel'dovich mechanism [22].

Figure 8 shows a completely different detonation onset although the section and dilution level remains

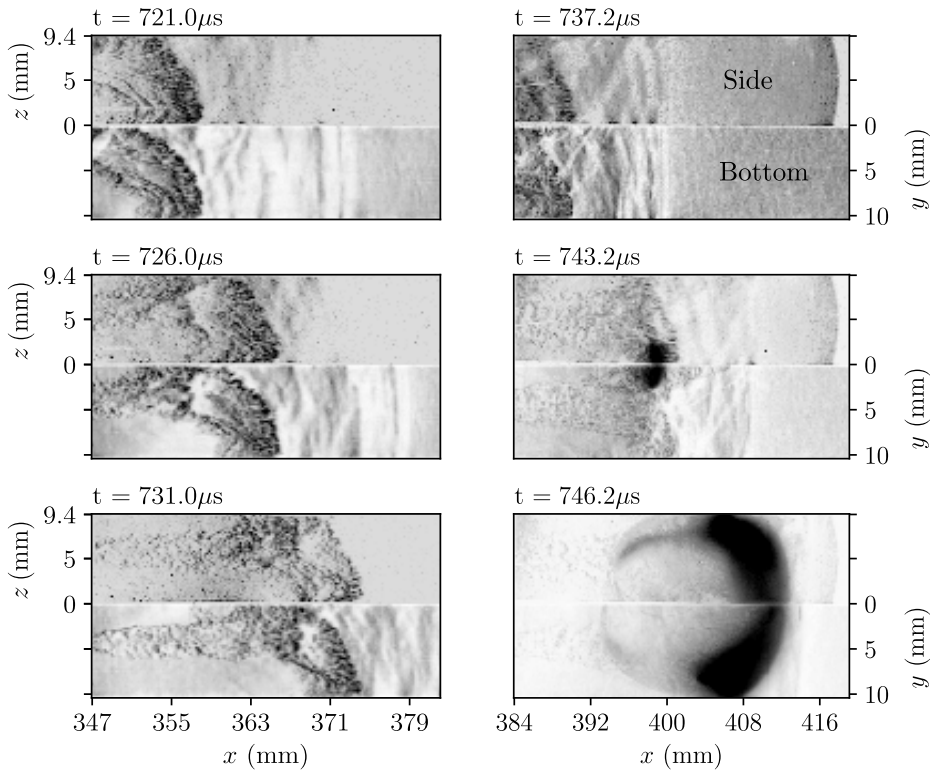

Figure 7: Detonation onset captured by a simultaneous *schlieren* visualization of an undiluted stoichiometric $2H_2$-O_2 flame. DDT happens through two sections: 347-384 mm and 384-421 mm from the closed end. t indicates the time elapsed from ignition.

unchanged. Confining an undiluted stoichiometric H_2-O_2 mixture is technically challenging. Due to its high mass diffusivity, fresh mixture can fill small regions/gaps outside the channel and burn without quenching as long as the size of the gap is of the order of or larger than the laminar thermal flame thickness of the mixture. The successive pressure build up from the flame acceleration process, sometimes causes slight bending of the polycarbonate allowing for fresh mixture to diffuse away. A sign of this phenomenon is visible in Fig. 8 as a reaction front that runs obliquely along a corner up to the leading precursor shock. We remark that this outcome was not observed with diluted mixtures likely due to actual flame quenching as a result of having larger thermal flame thicknesses for increasing N_2 dilution, or to the less significant pressure build-up during flame acceleration as a result of their lower expansion ratios. This detonation onset scenario may be more representative of the expected evolution during an accidental ignition event.

Figure 9 shows a typical transition episode for $\eta = 2$ which, as expected, occurs further away along the channel. The reduced image quality is due to the large number of tests performed before arriving at such far-from-ignition location and the fact that this region of the channel has been exposed to fully established detonations most of the time, hence very high pressures and temperatures, that diminish the optical quality of the polycarbonate walls. This results in strong diffusion of the collimated light beam, which worsens *schlieren* visualization. However, since the DDT evolution revealed different dynamics we deemed it appropriate to include the recorded frames in this manuscript.

The most notable differences are: (i) the flame is not followed by entrained unburned mixture. Instead, a finger-like corrugated flame generates curved pressures waves, forming a pre-heated zone in close proximity to itself but behind the leading precursor shock. This is visible at $t = 3278.5$ μs in Fig. 9.

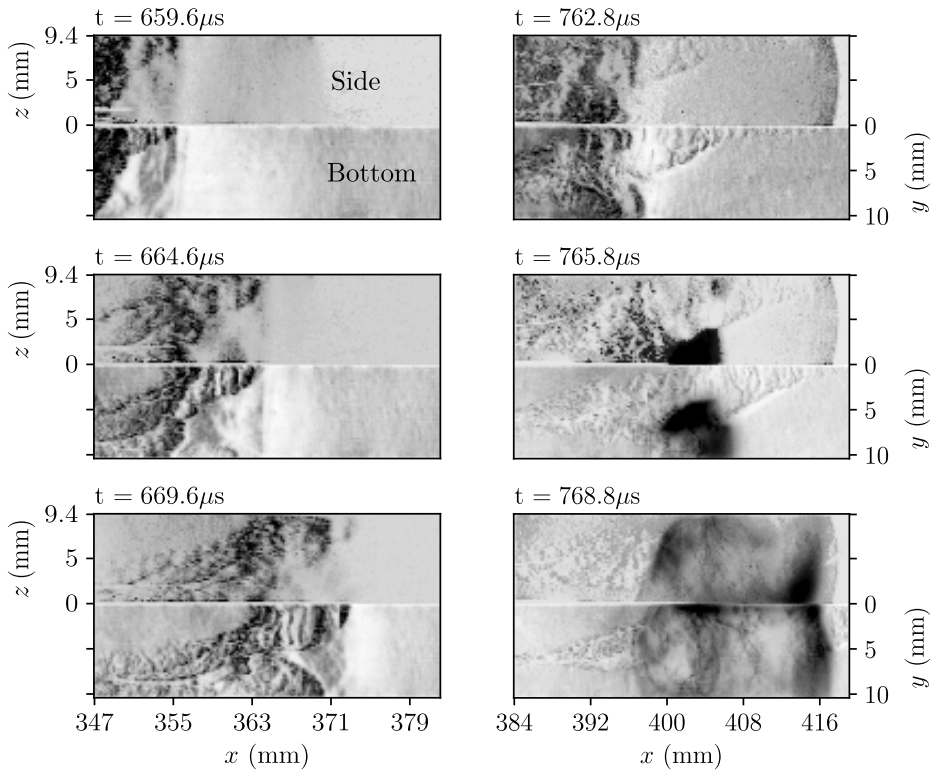

Figure 8: Alternative detonation onset captured by a simultaneous *schlieren* visualization of an undiluted stoichiometric $2H_2$-O_2 flame. DDT happens through two sections: 347-384 mm and 384-421 mm from the closed end. t indicates the time elapsed from ignition.

(ii) At t = 3444.2 μs, the initially curved shock flattens and the heating induced due to its interaction with the corners ignites symmetric oblique flames within the boundary layer that meet with the curved, corrugated reaction front that propagates along the channel's centerline. (iii) This shock-flame complex gradually starts to catch up with precursor shock, however, detonation onset occurs at the wall, close to the shock, before merging (see t = 3447.2 μs).

While flame-/shock- boundary layer interactions were found to be the main mechanisms leading to detonation onset across the dilutions studied, the nature of this interaction is of a different type for increasing dilution. The oblique flames propagate faster within corners through the pre-heated zone, unable to burn beyond this zone the flame is confined to propagate through the center of the channel further compressing the pre-heated zone prior to DDT. The overall detonation onset structures were more repeatable for η = 2 than for η = 0 as a result of the difficulties discussed above when trying to retain such highly-diffusive mixture within the channel. Lastly, for η = 2.5 the flame topology observed before leaving the optically accessible section is analog to that shown in Fig. 9; t = 3278.5 μs.

In Fig. 10 we summarize our data in a more quantitative manner showing the normalized run-up distances obtained, $x_{\mathrm{DDT}}/D_{\mathrm{h}}$, as a function of expansion ratio, σ, together with a DDT map (σ vs. β) delimiting the region where detonation onset was observed in our channel. Similar to the results reported for obstructed channels [23], σ is inversely proportional to x_{DDT}, i.e., mixtures with high σ are more prone to transit to detonation closer to their ignition point. On the other hand, for smooth 1-m long narrow channels, our results show that the transition boundary between DDT and no-DDT cases is raised two-fold when compared with channels with obstacles.

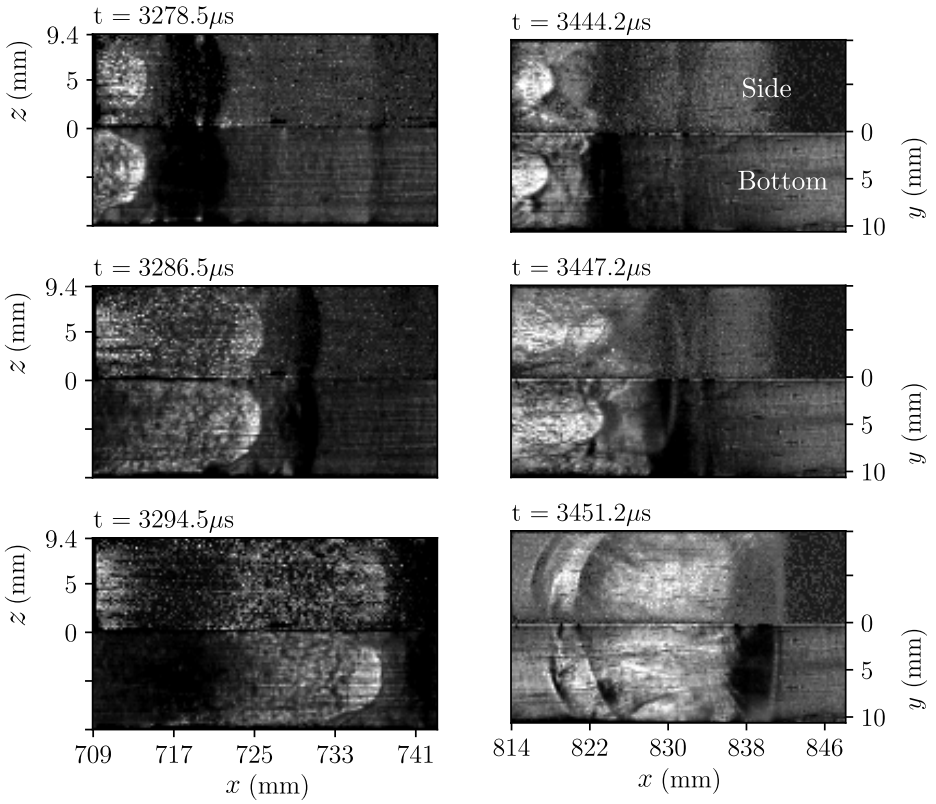

Figure 9: Detonation onset recorded by a simultaneous *schlieren* visualization of a stoichiometric $2H_2$-O_2-$2N_2$ flame. DDT happens through several sections. Here we show sections 709-746 mm and 814-851 mm from the closed end. t indicates the time elapsed from ignition.

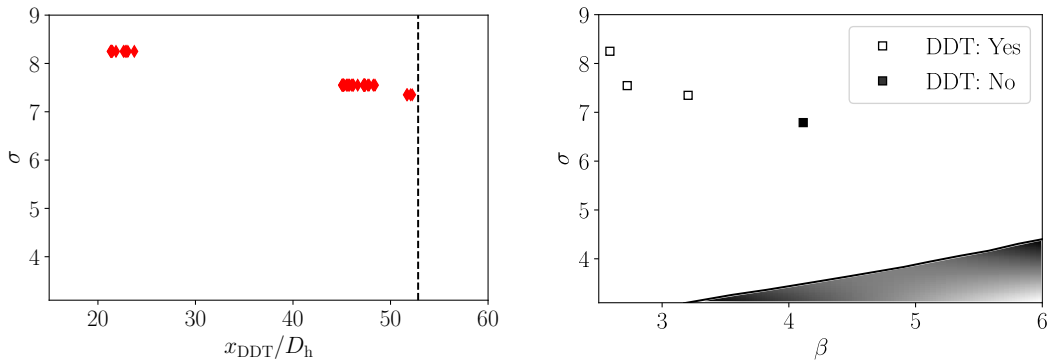

Figure 10: *Left:* normalized run up distance, x_{DDT}/D_h as a function of expansion ratio, σ, where $D_h = 2ab/(a+b)$ is the hydraulic diameter for a channel with a cross-sectional area $A = a \cdot b$; the vertical dotted line represents the end of the optically accessible region. *Right:* DDT map (expansion ratio, σ vs. Zel'dovich number, β); the solid line represents the DDT limit for channel with obstacles from [23]. Initial conditions: $p_0 = 100$ kPa, $T_0 = 300$ K and $2H_2+O_2+\eta N_2$.

4. CONCLUSION AND FUTURE WORK

A complete characterization of flame propagation, from ignition to transition to detonation, for N_2-diluted stoichiometric H_2-O_2 mixtures was carried out. The widely accepted symmetric assumptions during the very early stages of propagation were confirmed whereas complex asymmetric structures were unraveled and described during flame acceleration and detonation onset. The value of simultaneous two-direction high-speed schlieren visualization in providing unique insight into the true reacting front and wave topologies present during the entire DDT evolution was, for the first time, demonstrated. Flame-/shock- boundary layer interactions were a common theme in the cases considered. Future work will include the improvement of the optical quality for highly diluted mixtures and extraction of more quantitative information from our data such as the determination of critical flame speeds/acceleration rates as a function of expansion ratio, and the application of simple mathematical models capable of capturing the transition dynamics.

ACKNOWLEDGMENTS

This work was carried out in the Detonation Team of the Institut Pprime UPR 3346 CNRS. The authors gratefully acknowledge *l'École Doctorale SIMME*, and the contribution of the technical personnel, especially B. Carme, A. Claverie, J.C. Jouvanneau, and N. Papin. Financial support from the Agence Nationale de la Recherche Program JCJC (FASTD ANR-20-CE05-0011-01) is gratefully acknowledged.

REFERENCES

1. R. Zipf Jr, V. Gamezo, M. Sapko, W. Marchewka, K. Mohamed, E. Oran, D. Kessler, E. Weiss, J. Addis, F. Karnack, and D. Sellers, "Methane–air detonation experiments at niosh lake lynn laboratory," *Journal of Loss Prevention in the Process Industries*, vol. 26, no. 2, pp. 295–301, 2013.
2. G. Ciccarelli and S. Dorofeev, "Flame acceleration and transition to detonation in ducts," *Progress in energy and combustion science*, vol. 34, no. 4, pp. 499–550, 2008.
3. M. Liberman, M. Ivanov, A. Kiverin, M. Kuznetsov, A. Chukalovsky, and T. Rakhimova, "Deflagration-to-detonation transition in highly reactive combustible mixtures," *Acta Astronautica*, vol. 67, no. 7-8, pp. 688–701, 2010.
4. A. Y. Poludnenko, T. A. Gardiner, and E. S. Oran, "Spontaneous transition of turbulent flames to detonations in unconfined media," *Physical Review Letters*, vol. 107, no. 5, p. 054501, 2011.
5. T. Machida, M. Asahara, A. K. Hayashi, and N. Tsuboi, "Three-dimensional simulation of deflagration-to-detonation transition with a detailed chemical reaction model," *Combustion Science and Technology*, vol. 186, no. 10-11, pp. 1758–1773, 2014.
6. V. N. Gamezo, T. Ogawa, and E. S. Oran, "Flame acceleration and ddt in channels with obstacles: Effect of obstacle spacing," *Combustion and Flame*, vol. 155, no. 1-2, pp. 302–315, 2008.
7. V. N. Gamezo, A. M. Khokhlov, and E. S. Oran, "The influence of shock bifurcations on shock-flame interactions and ddt," *Combustion and flame*, vol. 126, no. 4, pp. 1810–1826, 2001.
8. E. Dziemińska and A. K. Hayashi, "Auto-ignition and DDT driven by shock wave–boundary layer interaction in oxyhydrogen mixture," *International Journal of Hydrogen Energy*, vol. 38, no. 10, pp. 4185–4193, 2013.
9. Y. Ballossier, F. Virot, and J. Melguizo-Gavilanes, "Flame propagation and acceleration in narrow channels: sensitivity to facility specific parameters," *Shock Waves*, 2021.
10. D. Goodwin, H. Moffat, and R. Speth, "Cantera: An object-oriented software toolkit for chemical kinetics, thermodynamics, and transport processes," 2009.
11. S. Browne, J. Ziegler, and J. Shepherd, "Numerical solution methods for shock and detonation jump conditions," *GALCIT report FM2006*, vol. 6, p. 90, 2008.
12. R. Mével, S. Javoy, F. Lafosse, N. Chaumeix, G. Dupré, and C. E. Paillard, "Hydrogen-nitrous oxide delay time: shock tube experimental study and kinetic modelling," *Proceedings of The Combustion Institute*, vol. 32, pp. 359–366, 2009.
13. R. Mével, S. Javoy, and G. Dupré, "A chemical kinetic study of the oxidation of silane by nitrous oxide, nitric oxide and oxygen," *Proceedings of The Combustion Institute*, vol. 33, pp. 485–492, 2011.
14. S. Bane, J. Ziegler, and J. Shepherd, "Development of one-step chemistry models for flame and ignition simulation," *GALCIT Report GALTCITFM*, vol. 2010, 2010.

15. C. Clanet and G. Searby, "On the "tulip flame" phenomenon," *Combustion and Flame*, vol. 105, no. 1-2, pp. 225–238, 1996.
16. V. Bychkov, V. Akkerman, G. Fru, A. Petchenko, and L.-E. Eriksson, "Flame acceleration in the early stages of burning in tubes," *Combustion and Flame*, vol. 150, no. 4, pp. 263–276, 2007.
17. D. M. Valiev, V. Akkerman, M. Kuznetsov, L.-E. Eriksson, C. K. Law, and V. Bychkov, "Influence of gas compression on flame acceleration in the early stage of burning in tubes," *Combustion and Flame*, vol. 160, no. 1, pp. 97–111, 2013.
18. H. Xiao, Q. Duan, L. Jiang, and J. Sun, "Effects of ignition location on premixed hydrogen/air flame propagation in a closed combustion tube," *International Journal of Hydrogen Energy*, vol. 39, no. 16, pp. 8557–8563, 2014.
19. X. Yang, M. Yu, K. Zheng, P. Luan, and S. Han, "On the propagation dynamics of lean h2/co/air premixed flame," *International Journal of Hydrogen Energy*, vol. 45, no. 11, pp. 7210–7222, 2020.
20. B. Ponizy, A. Claverie, and B. Veyssière, "Tulip flame-the mechanism of flame front inversion," *Combustion and Flame*, vol. 161, no. 12, pp. 3051–3062, 2014.
21. P. Krivosheyev, O. Penyazkov, and A. Sakalou, "Analysis of the final stage of flame acceleration and the onset of detonation in a cylindrical tube using high-speed stereoscopic imaging," *Combustion and Flame*, vol. 216, pp. 146–160, 2020.
22. Y. B. Zeldovich, "Regime classification of an exothermic reaction with nonuniform initial conditions," *Combustion and Flame*, vol. 39, no. 2, pp. 211–214, 1980.
23. S. B. Dorofeev, M. Kuznetsov, V. Alekseev, A. Efimenko, and W. Breitung, "Evaluation of limits for effective flame acceleration in hydrogen mixtures," *Journal of loss prevention in the process industries*, vol. 14, no. 6, pp. 583–589, 2001.